HHS Public Access

Author manuscript

Cancer Res. Author manuscript; available in PMC 2024 November 16.

Published in final edited form as:

Cancer Res. 2024 September 16; 84(18): 2954–2967. doi:10.1158/0008-5472.CAN-23-3628.

VPAC2 receptor signaling promotes pancreatic cancer cell growth and decreases the immunogenicity of the tumor microenvironment

Tenzin Passang[1,*], **Shuhua Wang**[1], **Hanwen Zhang**[1], **Fanyuan Zeng**[1], **Po-Chih Hsu**[1], **Wenxi Wang**[1], **Jian Ming Li**[1], **Yuan Liu**[2], **Sruthi Ravindranathan**[1], **Gregory B. Lesinski**[1,2], **Edmund K. Waller**[1,2,*]

[1]Department of Hematology and Medical Oncology, Winship Cancer Institute, Emory University, Atlanta, GA, USA.

[2]Winship Cancer Institute Emory University, Atlanta, GA, USA.

Abstract

Identifying the mechanisms underlying tumor growth and immune resistance is needed to treat pancreatic ductal adenocarcinoma (PDAC) effectively. The complexity of the tumor microenvironment (TME) suggests that the crosstalk between cells in the TME contributes to drug resistance and relapse in PDAC. We have previously determined that vasoactive intestinal peptide (VIP) is overexpressed in PDAC and that VIP receptors expressed on T cells are a targetable pathway that sensitizes PDAC to anti-PD1 therapy. In this study, we show that pancreatic cancer cells engage in autocrine VIP signaling through VIP-receptor 2 (VPAC2), and that high co-expression of VIP with VPAC2 leads to reduced relapse-free survival in PDAC patients. Mechanistically, we identified piwi-like RNA-mediated gene silencing2 (Piwil2) as a tumor-cell intrinsic protein downstream of VPAC2 that regulates cancer cell clonogenic growth. In addition, we discovered TGFβ-1 as a tumor-extrinsic inhibitor of T cell function induced by VPAC2 signaling. *In vivo*, knockout and knockdown of VPAC2 on PDAC cells led to reduced tumor growth rate and increased sensitivity to anti-PD-1 therapy in mouse models of PDAC with T cell-dependent anti-cancer immunity. Overall, these findings emphasize the implications of VIP/VPAC2 signaling in the PDAC tumor microenvironment and support the rationale for developing more potent VPAC2-specific antagonists.

[*]To whom correspondence should be addressed: tenzin.passang.fnu@emory.edu and ewaller@emory.edu.

Author contributions:

TP conceptualized the study, designed, and performed experiments, analyzed data, and wrote the manuscript. FZ assisted in the analysis of patient Kaplan-Meir plots. SW, HZ, CH, and JML assisted in some *in vivo* experiments and reviewed the manuscript. WW performed *in vitro* experiments and reviewed the manuscript. YL reviewed statistical analyses. SR provided input in experimental design, and GBL provided clinical samples and critically reviewed the manuscript. EKW conceptualized the study, edited the manuscript, and provided funding.

Disclosures of potential conflicts of interest

Intellectual property related to the use of peptide antagonists to vasoactive intestinal polypeptides to treat cancer is the subject of US patent applications with SR, TP, JML, and EKW listed as inventors. These patents have been licensed to Cambium Oncology, LLC. EKW is a co-founder and has equity in Cambium Oncology. A conflict-of-interest management plan has been reviewed and approved by Emory University.

Introduction

Pancreatic Ductal Adenocarcinoma (PDAC) is a highly lethal disease with a dismal 5-year overall survival rate of only 13% (1). By 2040, it is projected to become the second leading cause of cancer-related deaths in the United States (2). Approximately 80% of patients are diagnosed with non-resectable disease and are treated with radiation, chemotherapies, and/or targeted therapies, albeit with limited responses (3–5). PDAC has a highly desmoplastic and immunosuppressive TME with a paucity of effector T cells that limits the effectiveness of anti-CTLA-4 and anti-PD1 monotherapies (6–8), further emphasizing the need to understand the biological underpinnings that lead to immune resistance. Our group previously showed that the overexpression of vasoactive intestinal polypeptide (VIP) in PDAC contributes to the escape from immune surveillance (9).

VIP is a 28-amino acid peptide secreted by the enteric nervous system with known effects on peripheral vasodilation, cardiac contractility, and gut peristalsis (10). The biological actions of VIP are mediated by a family of G protein-coupled receptors, namely, VPAC1 and VPAC2 (11,12). In addition to its previously known functions, recent research indicates that VIP has anti-inflammatory effects on T cells, macrophages, and plasmacytoid dendritic cells (13–17). Our published data demonstrate that VIP expression by pancreatic cancer cells leads to paracrine signaling through VIP receptors on T cells, suppressing T cells, and increasing resistance to anti-PD-1 therapy (9). We observed that pancreatic cancer cells also express VPAC1 and VPAC2 and that the absence of VPAC2 on cancer cells results in delayed tumor growth rate *in vivo*, suggesting a potential autocrine function of VIP via VPAC2 (9).

A small body of literature has highlighted the growth-promoting properties of VIP in pancreatic cancer cell lines, which can be reversed by VIP-receptor antagonism (18–21). However, little is known about VIP receptors' intracellular signaling and downstream mechanisms in cancer. Moreover, there is a lack of clear understanding of how VIP-receptor signaling in pancreatic cancer cells contributes to the TME. In particular, limited studies have used clinically relevant orthotopic models to delineate the biological underpinnings of VIP receptors in PDAC.

This current work extends the understanding of how VIP receptors, mainly VPAC2, regulate tumor growth and modulate the TME. We found that higher VIP and VPAC2 expression correlate with worse relapse-free survival in PDAC patients compared to patients with low VIP and VPAC2 expression. Mechanistically, VPAC2 deletion reduces *in vitro* colony formation by decreasing stem-cell relating protein Piwil2. Furthermore, VPAC2 deletion leads to reduced TGFβ-1 through SP1 transcriptional regulation, linking VPAC2 to the modulation of non-tumor cell-autonomous effects in the TME. Data from *in vivo* tumor growth rates of knockout and knockdown of VPAC2 in mouse PDAC models confirms the role of VPAC2 signaling in promoting tumor growth and antagonizing sensitivity to anti-PD1 therapy. These findings position VPAC2 signaling at the intersection between tumor cell-intrinsic autocrine signaling to regulate growth and paracrine signaling to regulate immune cells in the TME.

Materials and Methods

Cell lines and reagents

MT5 and KPC.luc cells were generous gifts from Dr. Tuveson and Dr. Logsdon, respectively, and Dr. Pilon-Thomas provided Panc02 cells. KPC.luc cells are luciferase expressing murine pancreatic cancer cells derived from $Kras^{LSL\text{-}G12D}$, $p53^{-/-}$, Pdx1-cre spontaneous GEMM tumor model (22). MT5 cells are derived from $Kras^{LSL\text{-}G12D}$, $Trp53^{LSL\text{-}R270H}$, and Pdx1-cre GEMM model, and Panc02 cell lines from 3-methylcholanthrene-induced pancreatic tumors in C57BL/6 mice (23). MT5 cells were cultured in 1XRPMI medium, while KPC.luc and Panc02 were cultured in 1XDMEM medium. All media were supplemented with 10% FBS, 10 mM glutamine, and antibiotics. CRISPR/Cas9 VPAC2 knockout pools for Panc02 were purchased from Synthego (Redwood City, CA). KPC.luc cells were transduced with murine VPAC2 shRNA lentiviral particles (Santa Cruz Biotechnology) at a Multiplicity of Infection (MOI) of 20. CRISPR-KO VPAC2KO Panc02 cells were similarly transduced with VPAC2-overexpression lentiviral particles (Origene) at 50 MOI for the rescue experiment. Genetically modified cells were selected using puromycin and single-cell cloned via limiting dilution. All cells were tested negative for mycoplasma before experimentation.

Mice

The Institutional Animal Care and Use Committee at Emory University approved all experimental procedures. Female or male C57BL/6 (000664, the Jackson Laboratory) at 8–10 weeks of age were used for *in vivo* experiments. All animals were maintained according to guidelines, *The Guide for Care and Use of Laboratory Animals* (National Research Council).

Patients and samples

Formalin-fixed paraffin-embedded (FFPE) tissue blocks from pancreatic cancer patients were obtained under an IRB-approved protocol [IRB00102595] at the Winship Cancer Institute of Emory University.

Cell proliferation and Colony formation assay

Cell viability was assessed using the MTT cell proliferation kit I (Roche), following the manufacturer's instructions. The percentage of cell viability was normalized to 0 hour. For colony formation assays, 50–200 cells were plated in triplicates in 6-well plates and grown over 8 to 10 days. Following culture, cells were stained with 0.5% crystal violet for 30 minutes at room temperature (RT). Images were acquired and analyzed using CountPHICS. Colonies were manually counted for experiments if the average number of visible colonies for the groups was less than 50.

In vitro drug treatment

1 mM stock of VPAC2-specific antagonist (Pg 99–465 Trifluoroacetate, Bachem) and SP1 inhibitor (Plicamycin, MedChemExpress) were prepared in pyrogen-free water and DMSO respectively. Cells were treated with 10 μM VPAC2 antagonist or 0.5 μM plicamycin daily.

RNA Sequencing analysis of parental versus VPAC2 CRISPR-KO cells

RNA Sequencing were performed by Azenta Biosciences. Briefly, 1 million Panc02 cells were pelleted and submitted for bulk RNA-Sequencing analysis on the Illumina HiSeq 4000 platform. DESeq2 analysis on normalized gene counts was performed, followed by the Wald test to generate p-values and log2 fold changes. Genes with adjusted p-values of less than 0.01 and relative expression levels of log2 greater than −1 and 1 were considered significant. GSEA analysis was performed using Board Institute Hallmarks mouse gene sets on differentially expressed genes. Volcano plot and dot plots were generated using R-studio (Version 4.3.1).

Reverse Transcriptase Polymerase Chain Reaction (RT-PCR) and qRT-PCR

Total RNA was isolated using RNeasy Plus Micro Kit (Qiagen), and first-strand cDNA was prepared using an AMV RNA PCR kit (TaKaRa) from 1 mg of total RNA. PCR amplification for VPAC2 mRNA detection was carried out as previously described (9). For qPCR, PowerUp™ SYBR™ Green Master Mix was used. The PCR reaction was carried out in 96-well plates using the 7500 Fast Real-Time PCR System (Applied Biosystems). A melting curve analysis was performed for each sample to verify PCR specificity, and no template samples were used as a negative control. Fold changes were calculated by the ΔΔCt method by using GAPDH as a housekeeping gene. Primers used are detailed in Supplementary Table 2.

Proinflammatory cytokines and TGFβ immunoassay

0.3×10^6 KPC.luc, Panc02, and MT5 were cultured in 6 well plates with 2 mL of respective media. Cell-free media collected 72 hours after culture were tested for IL1-β, IL6, IL10 using the U-plex Proinflam Combo 1 for mouse (Cat. K15713K, MSD) and 3 TGFβ isoforms using TGFβ Combo cytokine plate for mouse (Cat. K15242K-1, MSD). Experiments were performed by Emory Multiplexed Immunoassay Core (Emory University). For specific TGFβ-1 detection in cell-free media, ELISA kit for mouse TGFβ-1 (Invitrogen, Cat. BMS608–4) was used.

T cell activation and function

Spleens were harvested from naïve C57BL/6 mice. T cells from splenocytes were isolated using a mouse pan-T cell isolation kit (Cat. 130-095-130, Miltenyl Biotec). 100,000 to 200,000 T cells were seeded in 96-well flat bottom plates coated with 0.1 μg/mL anti-mouse CD3e antibody (Cat. 16-0031-86, Invitrogen™) and cultured in PDAC conditioned media for 24 hours for CD69 expression analysis. For cytokine analysis, T cells were activated with 1 μg/mL anti-mouse CD3e antibody and cultured for 48 hours in T cell control media or PDAC conditioned media. Golgi plug (Cat. 51–2301KZ, BD) and Golgi stop (Cat. 51–2092KZ, BD) were added 4 hours before collection for flow cytometry analysis. All T cell cultures were done with 30 U/mL recombinant mouse IL-2. To assess phenotype after TGFβ-1 supplementation, recombinant TGFβ-1 at 2 ng/mL was added to the media. Depletion of latent TGF-β1 in the PDAC conditioned media was performed using purified anti-mouse LAP Antibody (Cat. 141402, Biolegend) compared to isotype control (Cat. 401402, Biolegend) as previously described (24).

Transcription Factor Profiling

Nuclear proteins were isolated from 70–80% confluent KPC.luc cells using Nuclear Extraction Kit (Cat. NPBP-29447, Novus) and quantified using Bradford protein assay. 9μg of total nuclear proteins from KPC cells was subjected for active transcription factor profiling (Cat. FA-1002, Signosis Inc.). Data was normalized to each plate using luminescence values from Gli-1 transcription factor that did not change between groups.

In vivo efficacy studies

For the subcutaneous model, 1×10^6 KPC.luc or Panc02 were injected in the right flank of female or male C57BL/6 mice. For anti-PD1 experiment using control transduced (control sh) or VPAC2 sh KPC.luc cells, 2×10^6 KPC.luc were injected in the right flank of male C57BL/6 mice. The study reached endpoint when the tumor volume reached 500 mm^3 or if the tumor was ulcerated. For NOD.Cg-Prkdc^{scid} Il2rg^{tm1Wjl}/SzJ (NSG) immunocompromised mice, 1×10^6 Panc02 or KPC.luc were injected subcutaneously and followed until tumor volume reached 1000 mm^3 and/or ulcerated. Vernier calipers were used to measure the tumor dimensions and the tumor volume was calculated using the formula: tumor volume = ½*(length × width × height). For the orthotopic KPC.luc model, mice were anesthetized, and the 200,000 KPC.luc cells were suspended in PBS: Matrigel (1:1) and injected in the tail of the pancreas during laparotomy. Tumor growth was monitored weekly for 25 days using IVIS bioluminescent imaging.

In vivo treatment

C57BL/6 mice were treated with 200 μg of murine antibodies to PD-1 (Clone RMP1–14) or isotype control (Clone 2A3) for 4 days (+7, +10, +14, +17) following tumor implantation. For the VPAC2 antagonist peptide experiment, female or male C57BL/6 mice were treated subcutaneously (s.c.) daily with 20 μg for ten days. Control mice received injections of 20 μg scrambled peptide. For depletion studies, anti-CD4 (Clone GK1.5) or anti-CD8 (Clone 2.43) antibodies were injected intraperitoneally (IP) at 200 μg per mouse on days −1 and at 100 μg +1, +3, +7, +11, +15) with respect to the date of tumor implantation. Antibodies were obtained from BioXcell and are detailed in Supplementary Table 1.

Histology

Pancreas harvested from mice with orthotopically implanted KPC.luc tumors were formalin-fixed and paraffin-embedded before being stained with H&E. All slides were dehydrated, cover-slipped, and scanned on Hamamatsu Nanozoomer 2.0 HT at 40x.

Immunofluorescence (IF)

FFPE PDAC tissues were deparaffinized, hydrated, and underwent antigen retrieval by boiling with 1X Trilogy for 15 minutes (Cell Marque-Trilogy Buffer). Permeabilization was performed using 0.3% Triton-X-100, followed by a blocking step with eBioscience™ high protein blocking buffer for 1 hour at RT. Primary antibodies for VIP, VPAC2, and CK19 (Suppl. Table 1) were applied with overnight incubation at 4 ℃. Secondary antibodies for anti-mouse IgG (H+L) conjugated with Alexa(R) 647 and anti-rabbit IgG (H+L) conjugated with Alexa(R) 488, and anti-goat conjugated with TRITC were applied and incubated for 1

hour at RT. Tissue slides were stained with 2 μg/mL Hoechst and imaged at Plan Fluor 40X objective on a BZ-X810 epifluorescence microscope (Keyence Corp). Multiple images were acquired and stitched using Keyence's image stitcher function and merged into a composite image using Fiji.

Statistical Analysis

For the comparison of one variable in more than two groups, one-way ANOVA followed by Dunnett's multiple comparison post-hoc test used. For the two groups comparison, an unpaired T test was used whereas multi-group comparison was performed using multiple unpaired T test with Welch's correction. A two-way ANOVA test with Bonferroni's correction for multiple comparisons was used to analyze tumor growth curves. For survival data from mouse studies, the Log-rank test was used. The Kaplan-Meier method with Log-rank tests was used to analyze survival data from PDAC patients. The Cox proportional hazard model estimated the hazard ratio for the Kaplan-Meier curves. R-squared values were generated from a linear regression model for PDAC TCGA dataset. P values less than 0.05 were considered significant. All statistical analyses were conducted using GraphPad Prism software, version 10.1.0.

Data Availability Statement

Bulk RNA Sequencing data is available under the GEO accession number (GSE248409). The data generated in this study are available upon request from the corresponding author.

Results

VIP and VPAC2 are co-expressed in human and murine pancreatic ductal adenocarcinoma.

To study the role of the VPAC2 receptor in PDAC, we first examined VPAC2 expression in human PDAC tissue. VPAC2 colocalized with the cancer epithelial cell marker, cytokeratin 19 (CK19) (Fig.1A). Moreover, CK19 positive cancerous ducts, but not CK19 positive normal ducts, expressed both VIP and VPAC2 (Fig.1B, Suppl. Fig.S1A). The relationship between VIP and VPAC2 was corroborated using a PDAC dataset from the Cancer Genome Atlas (TCGA) (n=149), where VIP mRNA expression was positively correlated with VPAC2 mRNA expression (R^2=0.34, p<0.0001) but not correlated with VPAC1 mRNA expression (Fig.1C and D). We found that VPAC2 mRNA expression trended towards higher median expression in Stage III/IV patients compared to Stage I and II. However, few stage III/IV patients are reported in the dataset (Suppl. Fig.S1B). Across the various point mutations of K-ras, that frequently occur in PDAC tumors, we observed a similar distribution of VPAC2 mRNA expression in K-ras-mutant versus wild type K-ras (Suppl. Fig.S1C). VPAC2 levels did not differ significantly between male and female patients (Fig.1E). To further study the clinical prognostic value of VIP and VPAC2, patients were stratified as Low_VIP versus High_VIP (cut-off value at 56, expression range 0 to 2149) and Low_VPAC2 versus High_VPAC2 (cut-off value at 22, expression range 0 to 297). The cut-off values for high and low expression were determined using methods previously published (25). Although multiple factors can impact patients' relapse-free survival (RFS) (26,27), we found significantly higher RFS for patients with low expression of both VIP

and VPAC2 (Low_VIP_VPAC2; 50 months) than patients with high VIP and VPAC2 (High_VIP_VPAC2) (18 months; HR:1.92, P <0.05), regardless of disease stage (Fig.1F, Supp. Fig.S1D). On the other hand, there was no significant difference in RFS for patients with low VIP and VPAC1 versus high VIP and VPAC1 (Supp. Fig.S1E). These data suggested the hypothesis that autocrine signaling of VIP via the VPAC2 receptor may regulate PDAC tumorgenicity and/or progression.

Decreased colony formation from disruption of VPAC2 on cancer cells is VIP dependent.

To explore the cell-intrinsic role of VPAC2 signaling on PDAC growth, we performed CRISPR-Cas9 deletion of VPAC2 on a murine PDAC cell line, Panc02. Lack of VPAC2 mRNA and VPAC2 protein in Panc02 cells, from now on termed VPAC2 knockout (VPAC2KO) (Fig.2A, Suppl. Fig.S2A and B), led to a 1.9-fold reduction in downstream CREB phosphorylation (47.4%±7.5 vs. 25.0%±5.5 in parental vs. VPAC2KO respectively) (Fig.2B) indicating the suppression of the VIP/VIP receptor signaling pathway, with no suppression in CRISPR-control cell line (Suppl. Fig.S2C). VPAC2KO cells had slightly delayed proliferation at 24 hours compared to parental cells (Fig.2C) similar to our published data (9), but subsequent growth rates were similar. We hypothesized that VPAC2KO cells may have impaired growth at low confluency due to absence of neighboring cell-to-cell contact. To test this hypothesis, we plated the cells at 100 cells per 6-well plate (9.6 cm^2/well) and found significantly fewer colonies with reduced colony size in VPAC2KO versus parental cells (27±4 vs. 62±7 colonies, respectively; Fig.2D). The suppressed colony formation was rescued upon VPAC2-overexpression (VPAC2-ORF) in VPAC2KO cells (37±5 colonies in control-ORF vector and 69±8 in rescue VPAC2-ORF; Fig.2E and F, Suppl. Fig.S2E). No significant difference in growth rate and colony number was found comparing parental and CRISPR-control cells (Suppl. Fig.S2D and E). Reduced colony formation was also observed by blocking VPAC2 pharmacologically with a VPAC2-specific antagonist in cultured Panc02 and MT5 murine PDAC cell lines, as well as following transient knockdown of VPAC2 using siRNA (Fig.2H and I, Suppl. Fig.S2F and G). Furthermore, neutralizing VIP in the supernatant using an anti-VIP antibody led to a significantly reduced number of colonies, similar to VPAC2 antagonist treatment (Fig.2H).

Decreased expression of *Piwil2*, a stem-cell-related gene downstream of VPAC2 signaling, decreased *in-vitro* colony formation.

To further examine the downstream consequences of VPAC2 signaling on pancreatic cancer cells, we performed bulk RNA sequencing on parental, CRISPR-control, and VPAC2KO Panc02 cells. Principal Component Analysis (PCA) indicated separate clustering for the parental vs. VPAC2KO samples, but not for parental vs. CRISPR-control, highlighting differences in a broad range of expressed genes between parental vs. VPAC2KO cells (Suppl. Fig.S3A and B). To account for genes in which expression may have been non-specifically affected due to CRISPR-Cas9 editing, we removed genes differentially expressed between parental and CRISPR-control samples (Suppl. Fig.S3C) from the differential gene analysis comparing parental and VPAC2KO cells. We found a total of 371 genes downregulated and 301 genes upregulated in VPAC2KO compared to parental cells (Fig.3A). Among the downregulated genes, Piwi Like RNA-Mediated Gene Silencing 2, commonly known as *Piwil2*, was significantly downregulated in VPAC2KO cells (log2

fold change −5.6; Fig.3A). We confirmed mRNA levels using qPCR, demonstrating reduced Piwil2 mRNA in the VPAC2KO cells, which increased by 2.8-fold following rescue of VPAC2 expression in the VPAC2KO Panc02 cell line (Fig.3B). We also observed a decrease in Piwil2 mRNA in the KPC.luc and MT5 cell line after blocking VPAC2 signaling with a VPAC2 antagonist (Fig.3C). To test the role of Piwil2 in survival of PDAC cells, we performed siRNA transfection targeting Piwil2. We found decreased colony formation compared to control transfected cells (Fig.3D, Suppl. Fig.S3D). Importantly, VPAC2 mRNA expression was positively correlated with Piwil2 mRNA expression in the human PDAC dataset ($R^2 = 0.1$, $p<0.01$; Fig.3E). Additionally, we identified other gene sets that were significantly downregulated in the VPAC2KO clone using Hallmarks gene sets GSEA analysis and observed myc targets as one of the significantly downregulated pathways compared to parental cells (Fig.3F, **bold**). GSEA analysis also showed other downregulated pathways, such as interferon alpha and gamma response pathways in the VPAC2KO Panc02 cells (Fig.3F). To examine this pathway, we interrogated two interferon-related markers, PDL1 and CD80 in cultured PDAC cells with or without interferon-gamma stimulation. We observed differential effects on the two markers with reduced PDL1 induction but increased CD80 expression in the VPAC2KO versus parental Panc02 cells following interferon-gamma treatment (Suppl. Fig.S3E and F).

VPAC2 regulates TGFβ-1 expression via SP1 and decreases T cell function.

In addition to the mRNA regulation of Piwil2 by VPAC2 receptor modulating tumor cell-intrinsic pathways, we were interested in whether the absence of VPAC2 signaling also alters the expression of cytokines that have immunosuppressive effects in the TME. Culture supernatants had low levels of the inflammation-related immunosuppressive cytokines IL6, IL10, and IL-1β, reported to be secreted by the PDAC cells (28,29), with levels of 0.5 pg/mL for IL10, 3–6 pg/mL IL6, and below detection level for IL-1β in the conditioned media from three PDAC cell lines (Suppl. Fig.S4A). In contrast, the levels of transforming growth factor beta (TGFβ) in culture supernatants, predominantly TGFβ-1, were elevated to >1000 pg/mL (Supp. Fig.S4B). Given the high TGFβ level may have an immunosuppressive role in the TME, we investigated whether VIP/VPAC2 signaling alters TGFβ levels. We first confirmed that the deletion of VPAC2 does not impact the expression of VIP as a potential positive feedback loop (Suppl. Fig.S4C and D). Knockout of VPAC2 in Panc02 (VPAC2KO) or knockdown of VPAC2 (VPAC2 sh) in KPC.luc both led to decreased expression of TGFβ-1 (Fig.4A, Suppl. Fig.S4E and F). TGFβ−3 also decreased in VPAC2KO Panc02 but was not affected by the knockdown of VPAC2 in KPC.luc cells (Suppl. Fig.S4E and F). Knockdown validations for VPAC2 in KPC.luc cell line are shown in supplementary Figures 3G & H. In addition, treatment with the VPAC2 antagonist decreased TGFβ-1 levels (Fig.4B). Decreased TGFβ-1 in VPAC2KO Panc02 cells did not correlate with consistent effects on EMT-related proteins, which led us to test if the secreted TGFβ-1 had paracrine effects on T cells. We cultured naïve T cells in PDAC-conditioned media from parental, VPAC2KO, and VPAC2-ORF rescue and assessed the effect of secreted factors on T cell activation (Fig.4C). T cells cultured in VPAC2KO-conditioned media (VPAC2KO-CM) had higher activation levels compared to parental-conditioned media (parental-CM) as measured by CD69 expression at 24 hours (22.8%±1.7 vs 18%±0.7) (Suppl. Fig.S4G). Moreover, the CD8+ T cells cultured in VPAC2KO-CM had approximately 10 percent

higher IFNγ expression (23.0%±1.6) than parental-CM (12.3%±0.4) and CRISPR-KO control CM (13.6%±1.2) (Fig.4D). The increased IFNγ expression levels on T cells cultured in VPAC2KO-CM were abrogated or reduced to levels similar to T cells in parental-CM when cultured in VPAC2-ORF rescueconditioned media (Rescue-CM) as well as upon addition of recombinant TGFβ-1 at 2 ng/mL to VPAC2KO-CM (Fig.4D). There was also a trend of increased TNFα and Ki67 in T cells cultured in VPAC2KO-CM, however, these differences were not significant compared to parental-CM (Suppl. Fig.S4H and I). Nevertheless, culturing T cells in Rescue-CM led to reduced expression of both TNFα and Ki67 on T cells when compared to VPAC2KO-CM (Suppl. Fig.S4H and I), further supporting the role of VPAC2 overexpression on T cell suppression in PDAC. To further assess the direct role of secreted TGFβ in the conditioned media from parental Panc02 cells, we depleted TGFβ in the parental conditioned media using the purified anti-mouse LAP antibody method as previously published (24). We saw that TGFβ depleted CM from parental cells as well as control-depleted VPAC2KO-CM resulted in significantly higher IFNγ expression in CD8+ T cells compared to anti-IgG depleted parental CM (Fig.4E, Suppl. Fig.S4J). The percentage of IFNγ expressing CD8+ T did not differ significantly between TGFβ depleted CM from parental cells and control-depleted VPAC2KO-CM. Together, these results indicate that TGFβ-1 in VPAC2-expressing cells contributes to decreased expression of Th1 effector cytokines.

Next, we profiled transcription factor expression using nuclear protein extracts from control and VPAC2 sh KPC.luc cells to elucidate the regulation of transcription factors downstream of VPAC2 signaling. We found reduced levels of GR/PR, SP1, ELK, OCT4, p53 and Brn-3 in the absence of VPAC2 (Fig.4F). We focused on the SP1 transcription factor given previous work indicating SP1 binding to the TGFβ-1 promoter region (30–33). We validated the reduced nuclear expression of SP1 via western blot in both KPC.luc VPAC2 sh and Panc02 VPAC2KO clones compared to control cell lines (Fig.4G). Furthermore, we found that treating PDAC cells with SP1 inhibitor, plicamycin, decreased TGFβ-1 (Fig.4H), representing a novel regulation of TGFβ-1 by SP1 downstream of VPAC2 signaling.

The absence of VPAC2 decreases tumor growth and increases sensitivity to anti-PD1 therapy in the subcutaneous PDAC model.

Next, we tested if the *in vitro* findings of tumor-intrinsic and tumor-extrinsic effects of VPAC2 signaling were recapitulated *in vivo*. We first inoculated control or VPAC2 sh KPC.luc to C57BL/6 mice and observed significantly slower growth rates in mice with VPAC2 sh tumors (**solid lines**, Fig.5A). The control transduced KPC.luc cell line (control sh) grew progressively in C57BL/6 mice (Fig.5A, **black line**). The two clones knocked down for VPAC2 (VPAC2 sh #5 and #8) grew at comparable rates to control sh tumors until day 10. At that time, the tumors began to shrink, leading to a significantly higher fraction of tumor-free mice at the end of the study (2/9 for mice with control sh tumors versus 6/10 and 7/10 mice with VPAC2 sh tumors) (Fig.5B and C). Tumor regression in the absence of VPAC2 was not observed when PDAC cells were implanted in the NSG mice, in which only slight delays in tumor growth were seen, suggestive of modest cell-intrinsic growth effects (**dashed lines**, Fig.5A and B). Next, we tested the sensitivity of control sh versus VPAC2 sh KPC.luc cells to anti-PD1 therapy in mice with injection of higher tumor cell

numbers. Treatment of control tumors with anti-PD1 therapy did not lead to tumor control, as shown by similar tumor growth rates in control tumors treated with isotype antibodies versus anti-PD1 treatment (Fig.5D). On the other hand, VPAC2 sh tumors had increased sensitivity to anti-PD1 therapy with significantly delayed tumor growth in comparison to anti-PD1 therapy in mice with control sh tumors (**orange line vs. green line**, Fig.5D). While VPAC2 sh tumors were smaller tumors compared to control sh tumors, differences were statistically not significant. As an alternative to the genetic approach, we tested the therapeutic efficacy of VPAC2-specific antagonist *in vivo* with or without anti-PD1 therapy in the KPC.luc model. VPAC2-antagonist treatment alone did not affect tumor growth but showed synergy with anti-PD1 therapy with significantly delayed tumor growth rate and prolonged survival in the combination group (Fig.5E and F).

Similar delayed growth was observed in the VPAC2KO Panc02 compared to parental Panc02 cells. However, all mice succumbed to the tumor with faster tumor growth rates in NSG mice than C57BL/6 mice (Fig.5D, Suppl. Fig.S5A). Notably, tumor volume at day 21 was higher in parental vs VPAC2KO Panc02 tumors in NSG mice, but parental tumors did not have higher expression of Ki67, a proliferation marker (Suppl. Fig.S5B–D). Next, we investigated the response of parental vs VPAC2KO Panc02 tumors to anti-PD-1 therapy. On average, the tumor growth rate of the parental cells was not altered by anti-PD1 therapy, consistent with previous reports (34,35), whereas anti-PD1 therapy suppressed tumor growth in mice with VPAC2KO tumors (Suppl. Fig.S5E). The median survival of mice challenged with the parental tumor was 27.5 days versus 50.5 days in those with VPAC2KO tumors following anti-PD1 therapy, albeit insignificant (p=0.2, Suppl. Fig.S5F). The survival advantage was significant in male mice, that have less anti-cancer immunity than female mice (36), in which no mice with parental tumors were rendered tumor-free with anti-PD1 therapy (0/5) versus 30% tumor-free male mice (3/10) with VPAC2KO tumors (Fig.5E and F). No significant differences in growth rates or survival were seen comparing parental versus VPAC2KO cells in female C57BL/6 mice (Suppl. Fig.S5G and H).

The absence of VPAC2 reduces tumor burden in a clinically relevant orthotopic model and increases T cell number and function in the tumor microenvironment.

The significant effects of VPAC2 in controlling the growth of subcutaneous KPC.luc in C57BL/6 mice led us to investigate further the role of VPAC2 signaling in a more clinically relevant orthotopic PDAC model. We surgically implanted control sh or VPAC2 sh clones of KPC.luc in the tail of the pancreas and monitored tumor growth *in vivo* by bioluminescence (BLI). We documented successful tumor engraftment 7 days following surgery (Suppl. Fig.S6A). In contrast to the control sh KPC.luc tumors, the VPAC2 knocked down clones (VPAC2 sh #8 and #5), show reduced tumor growth rates (Fig.6A). In fact, we found that one of the mice with initial engraftment of the VPAC2 sh#5 tumor had no detectable residual tumor at necropsy (Fig.6B, **red arrow**). These findings were further supported by lower tumor weights at day 26 for VPAC2 sh clones versus control sh KPC.luc tumors (tumor weights for control sh > VPAC2 sh#8 > VPAC2 sh#5) with no evident histological differences in the tumors after H&E staining (Fig.6C, Suppl. Fig.S6B). We did not observe any lung or liver metastasis at day 26 post tumor implantation in this model

(Suppl. Fig.S6C). To test whether the increased tumor control in the VPAC2 knockdown KPC.luc model was dependent on CD4+ or CD8+ T cells, we next performed depletion studies with anti-CD4 and anti-CD8 antibodies (Suppl. Fig.S6D). Once again, one of the mice transplanted with the VPAC2 sh clone in the isotype treatment group did not have a progressive tumor and had histologically normal pancreas tissue at necropsy (Fig.6E, **red arrow**). On average, mice with the VPAC2 sh tumors treated with isotype IgG had smaller tumors than control tumors. In contrast, treatment with anti-CD4 or anti-CD8 blockade led to the loss of tumor control as measured by increased total BLI flux and tumor weights (Fig.6D–F). Confirmation that the antibody treatment depleted CD4+ and CD8+ in the spleen and tumor at the end of the study are shown in Supplementary Figure 6E. Finally, we observed an increased number of CD4+ and CD8+ T cells infiltrating into VPAC2 sh KPC.luc tumors compared to control tumors (Fig.6G) with significantly fewer $PD1^{high}$ CD8+ T cells and a trend of more Ki67 positive CD8+ at the tumor site (Suppl. Fig.S6F–I). In addition, the CD8+ T cells in the VPAC2 sh tumors had increased effector phenotypes as measured by increased expression of both IFNγ and TNFα following *ex vivo* PMA stimulation (27.3%±10.5 in VPAC2 sh versus 6.5%±0.5 in Control) (Fig. 6H, Suppl. Fig.S6J). The delayed tumor growth rate in VPAC2 sh subcutaneous tumors with anti-PD1 therapy prompted us to repeat this experiment in an orthotopic model in which we tested anti-PD1 therapy in VPAC2 sh tumors. Mice with orthotopic VPAC2 sh KPC.luc tumors treated with anti-PD1 therapy had the lowest average tumor burden as measured by bioluminescence compared to all groups, albeit no significant difference between isotype and anti-PD1 group in VPAC2 sh tumors (Fig.6I). Nevertheless, when compared to control sh tumors treated with anti-PD1 therapy, treatment of VPAC2 sh tumors with anti-PD1 therapy led to a more significant decrease in tumor burden ($p<0.001$) compared with VPAC2 sh tumors treated with isotype-matched antibody ($p<0.01$) (Fig.6I).

Discussion

PDAC remains a challenging cancer with limited success of current treatment. The desmoplastic and immunosuppressive TME, constituting of a rich stromal compartment comprised of extracellular matrix, cancer-associated fibroblasts, immunosuppressive cell types such as MDSCs, regulatory T cells, and regulatory B cells, limits the entry and activity of anti-cancer T cells (6,7,37,38). In this study, we identify the VPAC2 signaling pathway as a novel vulnerability of PDAC critical to tumor growth and the generation of an immunosuppressive TME.

In tumors from PDAC patients and murine models of PDAC, we have previously demonstrated overexpression of VIP (9). Although, there have been other reports on VIP-receptor (VIP-R) signaling in PDAC, much of the prior work involved receptor activation with VIP or weak antagonism by VIPhyb (19–21). However, the downstream signaling pathways of VIP signaling on PDAC cells via VPAC1 and/or VPAC2 receptors remain to be elucidated. While studies have reported the expression of both VPAC1 and VPAC2 on human tumors (39,40), we observed a strong positive correlation of VIP expression with VPAC2, not VPAC1 expression in the PDAC TCGA dataset, leading us to hypothesize that VIP signals through VPAC2 on PDAC cells. We demonstrated that VPAC2 regulates tumor-intrinsic signaling by enhancing tumor growth *in vitro* and *in vivo*. Mechanistically, VPAC2

increases stem-cell-related Piwil2, which supports clonogenic proliferation *in vitro*. While several studies have demonstrated the tumor-promoting role of Piwil2 (41,42), there is no direct report of Piwil2 on the growth of PDAC cells. PIWI proteins interact with non-coding RNAs, commonly known as (piRNAs), in the nucleus, to regulate stem-cell maintenance and self-renewal genes (43). Consistent with the role of Piwil2 as a stem-cell marker, we observe reduced colony formation from single PDAC cells in the absence of VPAC2, representing a novel VPAC2 pathway to maintain cancer self-renewal. In addition, Piwil2 promotes c-myc expression by facilitating NME/NM23 nucleoside diphosphate kinase 2 binding to the c-myc promoter and subsequently enhancing tumor cell proliferation (44). Following the previous publication (44), GSEA analysis showed myc targets significantly downregulated in VPAC2KO cells compared to parental cells, which correlates with the downregulation of Piwil2. Alternatively, Piwil2 can regulate genes epigenetically to suppress apoptosis and promote cancer growth (45). Further mechanistic studies on how Piwil2 specifically mediates tumor-cell intrinsic growth following VPAC2 signaling in PDAC are necessary. However, these data together suggest the importance of the VIP/VPAC2 axis on positive regulation of tumor cell growth via Piwil2, thus implicating the autocrine signaling of VPAC2 on PDAC cells in a cell-intrinsic manner.

Beyond its tumor intrinsic role, VPAC2 modulates the activity of T cells in TME by regulating TGFβ-1 expression. Finding a protein with both tumor intrinsic and extrinsic roles in tumorigenesis is not novel, as illustrated by various groups describing the role of K-ras in regulating immunogenicity in the TME in addition to an oncogenic tumor-intrinsic role (46–49). We found that TGFβ-1 expression was highly elevated in media from PDAC cultures and that lower TGFβ-1 secretion in VPAC2-deficient PDAC cells promotes T cell activation. Transcriptionally, VPAC2 signaling enhances SP1 activity in the nucleus, promoting TGFβ-1 synthesis, as evidenced by reduced nuclear SP1 levels in VPAC2KO and VPAC2 sh cell lines and reduced TGFβ-1 expression after treatment with an SP1 inhibitor. While the transcriptional regulation of TGFβ-1 expression by SP1 has been previously reported in the literature (30–33), this is the first report that SP1 regulation downstream of VPAC2 signaling contributes to the malignant phenotype of PDAC. However, we cannot rule out the other transcription factors profiled from our assay including ELK, OCT4 and p53 as potential regulators downstream of VPAC2 signaling.

The non-cell autonomous effect of VPAC2-expressing tumor cells on the T cells was further supported by *in vivo* data with significantly lower tumor burden in recipients of VPAC2 sh subcutaneous and orthotopic KPC.luc tumors, which had increased sensitivity to anti-PD1 therapy compared to control tumors. This effect was dependent on the presence of CD4 and CD8 T cells, where the knockdown tumors had a higher percentage of cytokine-producing T cells infiltrating the tumor. Thus, our study presents a novel role for VPAC2 receptor on PDAC cells, promoting T cell exclusion and suppression in the TME in a paracrine fashion via TGFβ-1. TGFβ-1 is a pleiotropic cytokine and can have tumor-suppressing or promoting properties during PDAC progression (50–54). TGFβ signaling on cancer cells can induce apoptosis during the premalignant stage, whereas it promotes EMT transition and metastasis of established malignancy (54). However, the role of TGFβ as a negative regulator in the adaptive or innate immune system is well established and thus reflect an important pathway to control the immunogenicity in the TME (51,52,55). While our present

study shows modulation of TGFβ-1 secretion by cancer cells via VPAC2 signaling, alternate mechanisms may contribute to better tumor control by T cells in the VPAC2KO/sh tumors. Future directions can pursue whole secretome analysis by LC-MS/MS to identify additional soluble factors that interact with VIP/VPAC2 pathway. In addition to secreted factors, other mechanisms such as augmented interferon signaling in cancer cells can lead to the expression of inhibitory ligands on cancer cells that bind to inhibitory receptors on T cells and suppress T cell responses (56–59). PDL1 is a known inhibitory marker that binds to PD1 on T cells leading to T cell suppression. Our present work shows significantly reduced PDL1 induction in the VPAC2KO Panc02 cells versus parental Panc02 cells (Suppl. Fig.S3E and F), suggesting VPAC2 signaling may also interact with interferon-gamma receptor signaling to suppress immunogenicity in the TME. We previously published that blockade of VIP-receptors using ANT308, a high-affinity VIP-receptor antagonist, enhanced T cell activation and anti-cancer immunity in PDAC (9). Findings from our current study suggest that our previous report showing the anti-cancer activity of the VIP-receptor antagonist in PDAC models could be partially attributed to tumor-cell autonomous and non-tumor-cell autonomous effects from VPAC2 signaling in PDAC cells. Indeed, treatment of PDAC cell lines with ANT308 resulted in similar effects on colony formation as were seen using the VPAC2 inhibitor. In conclusion, our study elucidates the importance of autocrine VIP signaling via VPAC2 as a potential resistance mechanism to promote tumor growth in a tumor cell-intrinsic and extrinsic manner. VPAC2 regulates Piwil2 and TGFβ-1 to increase cancer cell clonogenic growth and T cell suppression, respectively, leading to reduced tumor control in PDAC (Fig.7). Elucidating the mechanisms of VIP-receptor signaling in PDAC provides new insights to optimize the clinical development of drugs targeting this highly aggressive cancer.

Supplementary Material

Refer to Web version on PubMed Central for supplementary material.

Acknowledgements

The authors thank patients for their tissue samples. The authors also thank Maggie Phillips from Emory University for teaching the procedures of orthotopic surgeries, the shared resources at Emory University, namely Emory Flow Cytometry Core (EFCC), Cancer Animal Models Shared Resource (CAMS), Cancer Tissue Pathology Core (CTP), and Integrated Cellular Imaging Core (ICI), that provided services or instruments at subsidized cost to conduct some of the reported experiments. The authors thank Dr. Tuveson (Cold Spring Harbor Laboratory, Cold Spring Harbor, NY), Dr. Logsdon (MD Anderson Cancer Center, Houston, Texas), and Dr. Pilon-Thomas (H. Lee Moffitt Cancer Center, Tampa, FL) for providing the PDAC cell lines. The data regarding VIP or VPAC1 mRNA and VPAC2 mRNA levels in human tumors discussed here are based upon data generated by The Cancer Genome Atlas Research Network: https://www.cancer.gov/tcga. This work was supported in by Katz Foundation funding.

References

1. Siegel RL, Giaquinto AN, Jemal A. Cancer statistics, 2024. CA Cancer J Clin 2024;74:12–49 [PubMed: 38230766]
2. Rahib L, Wehner MR, Matrisian LM, Nead KT. Estimated Projection of US Cancer Incidence and Death to 2040. JAMA Netw Open 2021;4:e214708 [PubMed: 33825840]
3. Mizrahi JD, Surana R, Valle JW, Shroff RT. Pancreatic cancer. Lancet 2020;395:2008–20 [PubMed: 32593337]

4. Park W, Chawla A, O'Reilly EM. Pancreatic Cancer: A Review. JAMA 2021;326:851–62 [PubMed: 34547082]
5. Fang YT, Yang WW, Niu YR, Sun YK. Recent advances in targeted therapy for pancreatic adenocarcinoma. World J Gastrointest Oncol 2023;15:571–95 [PubMed: 37123059]
6. Ho WJ, Jaffee EM, Zheng L. The tumour microenvironment in pancreatic cancer - clinical challenges and opportunities. Nat Rev Clin Oncol 2020;17:527–40 [PubMed: 32398706]
7. Sherman MH, Beatty GL. Tumor Microenvironment in Pancreatic Cancer Pathogenesis and Therapeutic Resistance. Annu Rev Pathol 2023;18:123–48 [PubMed: 36130070]
8. Halbrook CJ, Lyssiotis CA, Pasca di Magliano M, Maitra A. Pancreatic cancer: Advances and challenges. Cell 2023;186:1729–54 [PubMed: 37059070]
9. Ravindranathan S, Passang T, Li JM, Wang S, Dhamsania R, Ware MB, et al. Targeting vasoactive intestinal peptide-mediated signaling enhances response to immune checkpoint therapy in pancreatic ductal adenocarcinoma. Nat Commun 2022;13:6418 [PubMed: 36302761]
10. Iwasaki M, Akiba Y, Kaunitz JD. Recent advances in vasoactive intestinal peptide physiology and pathophysiology: focus on the gastrointestinal system. F1000Res 2019;8
11. Dickson L, Finlayson K. VPAC and PAC receptors: From ligands to function. Pharmacol Ther 2009;121:294–316 [PubMed: 19109992]
12. Harmar AJ, Fahrenkrug J, Gozes I, Laburthe M, May V, Pisegna JR, et al. Pharmacology and functions of receptors for vasoactive intestinal peptide and pituitary adenylate cyclase-activating polypeptide: IUPHAR review 1. Br J Pharmacol 2012;166:4–17 [PubMed: 22289055]
13. Delgado M, Pozo D, Ganea D. The significance of vasoactive intestinal peptide in immunomodulation. Pharmacol Rev 2004;56:249–90 [PubMed: 15169929]
14. Petersen CT, Li JM, Waller EK. Administration of a vasoactive intestinal peptide antagonist enhances the autologous anti-leukemia T cell response in murine models of acute leukemia. Oncoimmunology 2017;6:e1304336 [PubMed: 28638725]
15. Villanueva-Romero R, Gutierrez-Canas I, Carrion M, Gonzalez-Alvaro I, Rodriguez-Frade JM, Mellado M, et al. Activation of Th lymphocytes alters pattern expression and cellular location of VIP receptors in healthy donors and early arthritis patients. Sci Rep 2019;9:7383 [PubMed: 31089161]
16. Kittikulsuth W, Nakano D, Kitada K, Uyama T, Ueda N, Asano E, et al. Vasoactive intestinal peptide blockade suppresses tumor growth by regulating macrophage polarization and function in CT26 tumor-bearing mice. Sci Rep 2023;13:927 [PubMed: 36650220]
17. Sakamoto K, Kittikulsuth W, Miyako E, Steeve A, Ishimura R, Nakagawa S, et al. The VIPR2-selective antagonist KS-133 changes macrophage polarization and exerts potent anti-tumor effects as a single agent and in combination with an anti-PD-1 antibody. PLoS One 2023;18:e0286651 [PubMed: 37405999]
18. Estival A, Mounielou P, Trocheris V, Scemama JL, Clemente F, Hollande E, et al. Presence of VIP receptors in a human pancreatic adenocarcinoma cell line. Modulation of the cAMP response during cell proliferation. Biochem Biophys Res Commun 1983;111:958–63 [PubMed: 6301493]
19. Jiang S, Kopras E, McMichael M, Bell RH Jr., Ulrich CD 2nd. Vasoactive intestinal peptide (VIP) stimulates in vitro growth of VIP-1 receptor-bearing human pancreatic adenocarcinoma-derived cells. Cancer Res 1997;57:1475–80 [PubMed: 9108448]
20. Zia H, Leyton J, Casibang M, Hau V, Brenneman D, Fridkin M, et al. (N-stearyl, norleucine17) VIP hybrid inhibits the growth of pancreatic cancer cell lines. Life Sci 2000;66:379–87 [PubMed: 10670826]
21. Rekasi Z, Varga JL, Schally AV, Halmos G, Armatis P, Groot K, et al. Antagonists of growth hormone-releasing hormone and vasoactive intestinal peptide inhibit tumor proliferation by different mechanisms: evidence from in vitro studies on human prostatic and pancreatic cancers. Endocrinology 2000;141:2120–8 [PubMed: 10830299]
22. Ware MB, Phillips M, McQuinn C, Zaidi MY, Knochelmann HM, Greene E, et al. Dual IL-6 and CTLA-4 blockade regresses pancreatic tumors in a T cell- and CXCR3-dependent manner. JCI Insight 2023;8

23. Corbett TH, Roberts BJ, Leopold WR, Peckham JC, Wilkoff LJ, Griswold DP Jr., et al. Induction and chemotherapeutic response of two transplantable ductal adenocarcinomas of the pancreas in C57BL/6 mice. Cancer Res 1984;44:717–26 [PubMed: 6692374]
24. Oida T, Weiner HL. Murine CD4 T cells produce a new form of TGF-beta as measured by a newly developed TGF-beta bioassay. PLoS One 2011;6:e18365 [PubMed: 21494571]
25. Nagy A, Munkacsy G, Gyorffy B. Pancancer survival analysis of cancer hallmark genes. Sci Rep 2021;11:6047 [PubMed: 33723286]
26. Aoyama T, Yamamoto N, Kamiya M, Murakawa M, Tamagawa H, Sawazaki S, et al. The Lymph Node Ratio Is an Independent Prognostic Factor in Pancreatic Cancer Patients Who Receive Curative Resection Followed by Adjuvant Chemotherapy. Anticancer Res 2018;38:4877–82 [PubMed: 30061263]
27. Truty MJ, Kendrick ML, Nagorney DM, Smoot RL, Cleary SP, Graham RP, et al. Factors Predicting Response, Perioperative Outcomes, and Survival Following Total Neoadjuvant Therapy for Borderline/Locally Advanced Pancreatic Cancer. Ann Surg 2021;273:341–9 [PubMed: 30946090]
28. Das S, Shapiro B, Vucic EA, Vogt S, Bar-Sagi D. Tumor Cell-Derived IL1beta Promotes Desmoplasia and Immune Suppression in Pancreatic Cancer. Cancer Res 2020;80:1088–101 [PubMed: 31915130]
29. Zhang Y, Yan W, Collins MA, Bednar F, Rakshit S, Zetter BR, et al. Interleukin-6 is required for pancreatic cancer progression by promoting MAPK signaling activation and oxidative stress resistance. Cancer Res 2013;73:6359–74 [PubMed: 24097820]
30. Geiser AG, Busam KJ, Kim SJ, Lafyatis R, O'Reilly MA, Webbink R, et al. Regulation of the transforming growth factor-beta 1 and -beta 3 promoters by transcription factor Sp1. Gene 1993;129:223–8 [PubMed: 8325508]
31. Li JM, Datto MB, Shen X, Hu PP, Yu Y, Wang XF. Sp1, but not Sp3, functions to mediate promoter activation by TGF-beta through canonical Sp1 binding sites. Nucleic Acids Res 1998;26:2449–56 [PubMed: 9580699]
32. Verrecchia F, Rossert J, Mauviel A. Blocking sp1 transcription factor broadly inhibits extracellular matrix gene expression in vitro and in vivo: implications for the treatment of tissue fibrosis. J Invest Dermatol 2001;116:755–63 [PubMed: 11348466]
33. Botella LM, Sanchez-Elsner T, Sanz-Rodriguez F, Kojima S, Shimada J, Guerrero-Esteo M, et al. Transcriptional activation of endoglin and transforming growth factor-beta signaling components by cooperative interaction between Sp1 and KLF6: their potential role in the response to vascular injury. Blood 2002;100:4001–10 [PubMed: 12433697]
34. Kinkead HL, Hopkins A, Lutz E, Wu AA, Yarchoan M, Cruz K, et al. Combining STING-based neoantigen-targeted vaccine with checkpoint modulators enhances antitumor immunity in murine pancreatic cancer. JCI Insight 2018;3
35. Ma Y, Li J, Wang H, Chiu Y, Kingsley CV, Fry D, et al. Combination of PD-1 Inhibitor and OX40 Agonist Induces Tumor Rejection and Immune Memory in Mouse Models of Pancreatic Cancer. Gastroenterology 2020;159:306–19 e12 [PubMed: 32179091]
36. Kwon H, Schafer JM, Song NJ, Kaneko S, Li A, Xiao T, et al. Androgen conspires with the CD8(+) T cell exhaustion program and contributes to sex bias in cancer. Sci Immunol 2022;7:eabq2630 [PubMed: 35420889]
37. Darvin P, Toor SM, Sasidharan Nair V, Elkord E. Immune checkpoint inhibitors: recent progress and potential biomarkers. Exp Mol Med 2018;50:1–11
38. Siegel RL, Miller KD, Wagle NS, Jemal A. Cancer statistics, 2023. Ca-Cancer J Clin 2023;73:17–48 [PubMed: 36633525]
39. Schulz S, Rocken C, Mawrin C, Weise W, Hollt V, Schulz S. Immunocytochemical identification of VPAC1, VPAC2, and PAC1 receptors in normal and neoplastic human tissues with subtype-specific antibodies. Clin Cancer Res 2004;10:8235–42 [PubMed: 15623599]
40. Schulz S, Mann A, Novakhov B, Piggins HD, Lupp A. VPAC2 receptor expression in human normal and neoplastic tissues: evaluation of the novel MAB SP235. Endocr Connect 2015;4:18–26 [PubMed: 25504760]

41. Han YN, Li Y, Xia SQ, Zhang YY, Zheng JH, Li W. PIWI Proteins and PIWI-Interacting RNA: Emerging Roles in Cancer. Cell Physiol Biochem 2017;44:1–20 [PubMed: 29130960]
42. Liu Y, Dou M, Song X, Dong Y, Liu S, Liu H, et al. The emerging role of the piRNA/piwi complex in cancer. Mol Cancer 2019;18:123 [PubMed: 31399034]
43. Girard A, Sachidanandam R, Hannon GJ, Carmell MA. A germline-specific class of small RNAs binds mammalian Piwi proteins. Nature 2006;442:199–202 [PubMed: 16751776]
44. Yao Y, Li C, Zhou X, Zhang Y, Lu Y, Chen J, et al. PIWIL2 induces c-Myc expression by interacting with NME2 and regulates c-Myc-mediated tumor cell proliferation. Oncotarget 2014;5:8466–77 [PubMed: 25193865]
45. Zhang Y, Zheng X, Tan H, Lu Y, Tao D, Liu Y, et al. PIWIL2 suppresses Siah2-mediated degradation of HDAC3 and facilitates CK2alpha-mediated HDAC3 phosphorylation. Cell Death Dis 2018;9:423 [PubMed: 29555935]
46. Muzumdar MD, Chen PY, Dorans KJ, Chung KM, Bhutkar A, Hong E, et al. Survival of pancreatic cancer cells lacking KRAS function. Nat Commun 2017;8:1090 [PubMed: 29061961]
47. Hamarsheh S, Gross O, Brummer T, Zeiser R. Immune modulatory effects of oncogenic KRAS in cancer. Nat Commun 2020;11:5439 [PubMed: 33116132]
48. Ischenko I, D'Amico S, Rao M, Li J, Hayman MJ, Powers S, et al. KRAS drives immune evasion in a genetic model of pancreatic cancer. Nat Commun 2021;12:1482 [PubMed: 33674596]
49. Mahadevan KK, McAndrews KM, LeBleu VS, Yang S, Lyu H, Li B, et al. KRAS(G12D) inhibition reprograms the microenvironment of early and advanced pancreatic cancer to promote FAS-mediated killing by CD8(+) T cells. Cancer Cell 2023;41:1606–20 e8 [PubMed: 37625401]
50. Ijichi H, Chytil A, Gorska AE, Aakre ME, Fujitani Y, Fujitani S, et al. Aggressive pancreatic ductal adenocarcinoma in mice caused by pancreas-specific blockade of transforming growth factor-beta signaling in cooperation with active Kras expression. Genes Dev 2006;20:3147–60 [PubMed: 17114585]
51. Principe DR, DeCant B, Mascarinas E, Wayne EA, Diaz AM, Akagi N, et al. TGFbeta Signaling in the Pancreatic Tumor Microenvironment Promotes Fibrosis and Immune Evasion to Facilitate Tumorigenesis. Cancer Res 2016;76:2525–39 [PubMed: 26980767]
52. Batlle E, Massague J. Transforming Growth Factor-beta Signaling in Immunity and Cancer. Immunity 2019;50:924–40 [PubMed: 30995507]
53. Principe DR, Timbers KE, Atia LG, Koch RM, Rana A. TGFbeta Signaling in the Pancreatic Tumor Microenvironment. Cancers (Basel) 2021;13
54. David CJ, Huang YH, Chen M, Su J, Zou Y, Bardeesy N, et al. TGF-beta Tumor Suppression through a Lethal EMT. Cell 2016;164:1015–30 [PubMed: 26898331]
55. Thomas DA, Massague J. TGF-beta directly targets cytotoxic T cell functions during tumor evasion of immune surveillance. Cancer Cell 2005;8:369–80 [PubMed: 16286245]
56. Benci JL, Xu B, Qiu Y, Wu TJ, Dada H, Twyman-Saint Victor C, et al. Tumor Interferon Signaling Regulates a Multigenic Resistance Program to Immune Checkpoint Blockade. Cell 2016;167:1540–54 e12 [PubMed: 27912061]
57. Jacquelot N, Yamazaki T, Roberti MP, Duong CPM, Andrews MC, Verlingue L, et al. Sustained Type I interferon signaling as a mechanism of resistance to PD-1 blockade. Cell Res 2019;29:846–61 [PubMed: 31481761]
58. Burks J, Fleury A, Livingston S, Smith JP. ISG15 pathway knockdown reverses pancreatic cancer cell transformation and decreases murine pancreatic tumor growth via downregulation of PDL-1 expression. Cancer Immunol Immunother 2019;68:2029–39 [PubMed: 31709456]
59. Espinet E, Gu Z, Imbusch CD, Giese NA, Buscher M, Safavi M, et al. Aggressive PDACs Show Hypomethylation of Repetitive Elements and the Execution of an Intrinsic IFN Program Linked to a Ductal Cell of Origin. Cancer Discov 2021;11:638–59 [PubMed: 33060108]

Significance

Autocrine VIP signaling via VPAC2 promotes cancer cell growth and inhibits T cell function in pancreatic ductal adenocarcinoma, making it a potential therapeutic target in PDAC.

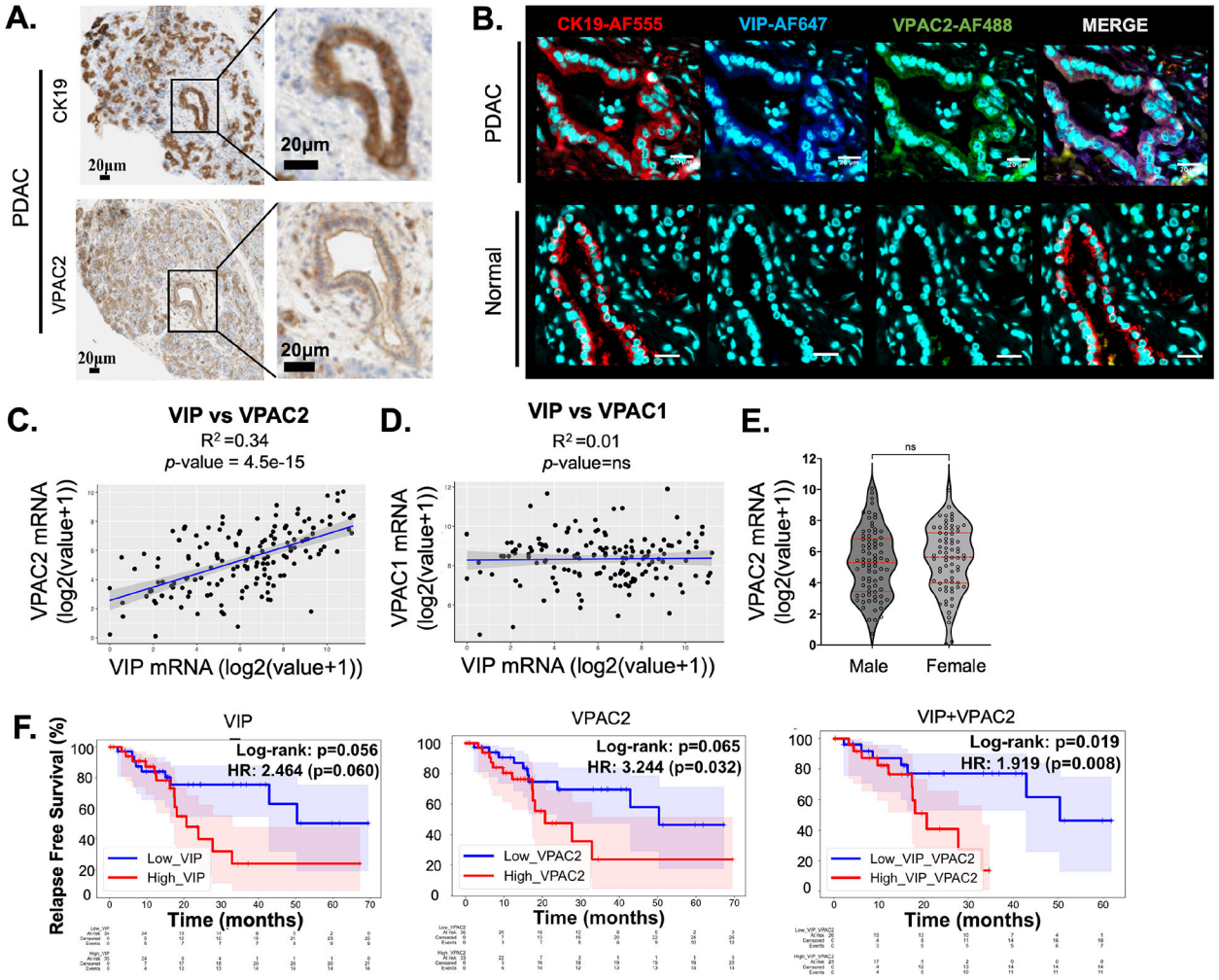

Figure1.

VIP and VPAC2 is co-expressed in pancreatic ductal adenocarcinoma. **(A)** Immunohistochemistry staining on PDAC tissue for VPAC2 and cytokeratin 19 (CK19). **(B)** Immunofluorescence on PDAC tissue showing expression of VIP (Mouse anti-VIP antibody), VPAC2 (Rabbit anti-VPAC2) and CK19 (Goat anti-CK19). Anti-Goat Alexa (R) 555, anti-mouse Alexa(R) 647 and anti-rabbit Alexa (R) 488 secondary antibodies was used for fluorescence detection. CK19 staining is shown for pancreatic cancer ductal cells. Scale bar 20 μm. **(C)** Linear regression model for VIP and VPAC2 mRNA expression and **(D)** VIP and VPAC1 mRNA expression from TCGA Pancreatic Cancer dataset (n=149). **(E)** VPAC2 mRNA expression between male and female PDAC patients, extracted from TCGA Pancreatic Cancer dataset. **(F)** Relapse free survival for PDAC patients with high and low expression of VIP and VPAC2. The shaded colors below and above the survival curves correspond to 95% confidence interval for the respective patient groups. For survival analysis, Log-rank test was performed for survival difference between patients. Hazard ratio (HR) was estimated by Cox proportional hazard model.

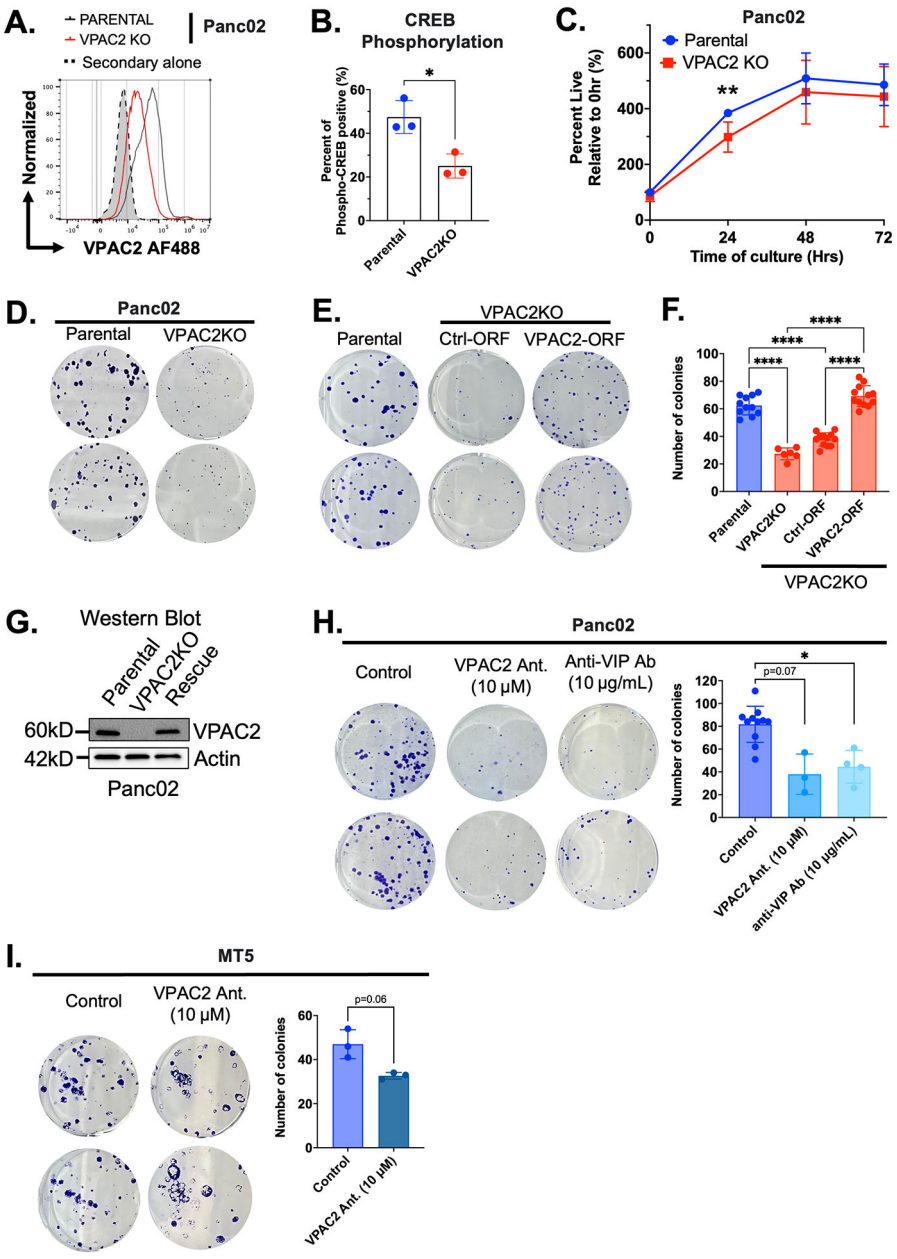

Figure2.

Absence of VIP and VPAC2 signaling leads to decreased colony formation *in vitro*. **(A)** Flow cytometry for surface expression detection of VPAC2 using rabbit polyclonal anti-VPAC2 antibody and **(B)** levels of phosphorylated CREB in parental Panc02 versus CRISPR-edited VPAC2KO Panc02 cells. **(C)** MTT assay showing growth of Panc02 cells over 72 hours (n=3). **(D)** Representative pictures of crystal violet colony assay for parental Panc02 and VPAC2KO Panc02 cells and **(E)** VPAC2-ORF rescue Panc02 cells. Cells were stained with crystal violet stain after 8 days of culture. **(F)** Colonies were counted using countPHICS software. **(G)** Western blot confirmation of VPAC2KO and VPAC2 rescue in VPAC2KO Panc02 cells using polyclonal anti-VPAC2 antibody. Crystal violet colony assay for **(H)** Panc02 and **(I)** MT5 treated with VPAC2-specific peptide-based antagonist (10

μM) and anti-VIP antibody (10 μg/mL). Cells were treated daily for 8 days with VPAC2 antagonist (VPAC2 Ant.) versus a single treatment of anti-VIP antibody. Data are presented as bar graphs or line plots ± standard deviation (SD). For B and I, two-tailed unpaired t test was used. For F and H, one-way ANOVA test following by Dunnet's multiple comparison post-hoc test was performed. *$p<0.05$, ****$p<0.0001$.

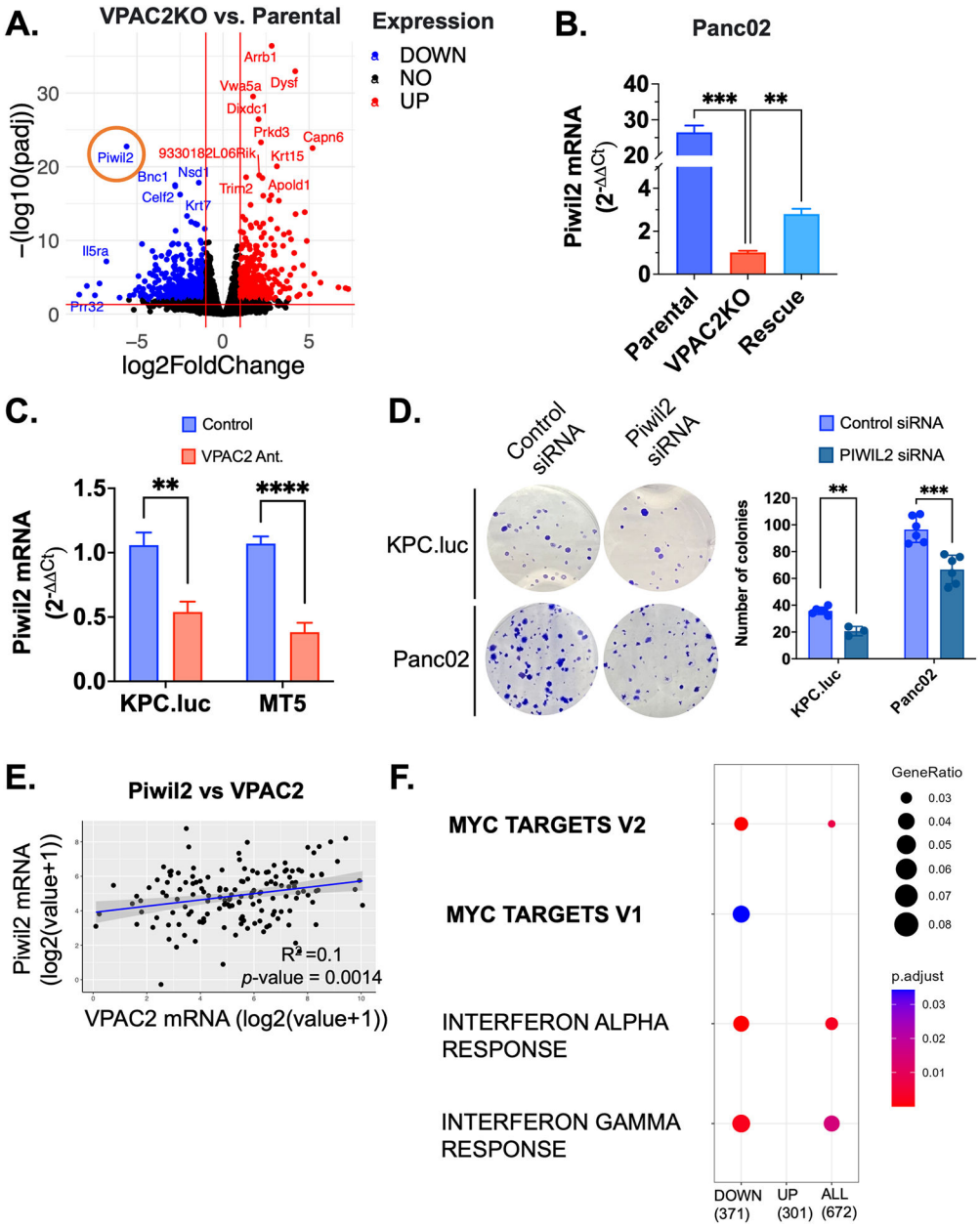

Figure 3.

Decreased transcription of the stem-cell related gene, *Piwil2*, downstream of VPAC2 signaling leads to decreased colony formation *in-vitro*. **(A)** Volcano plot of significantly downregulated (blue) and upregulated (red) genes between parental and VPAC2KO Panc02 cells from RNA Sequencing analysis. Piwil2 (circled in orange) were one of the top 50 genes downregulated in the VPAC2KO compared to parental cells. **(B)** qRT-PCR confirmation of Piwil2 mRNA expression in VPAC2KO and VPAC2-rescue Panc02 cells versus parental Panc02 cells (n=5). **(C)** qRT-PCR for Piwil2 mRNA expression in KPC.luc and MT5 after treatment of cells for 3 days with VPAC2-antagonist *in vitro* (n=8). **(D)** Crystal violet colony assay for KPC.luc and Panc02 cells. Cells were transfected with control or Piwil2-targeting siRNA for 2 days. siRNA transfected cells were plated at 50–100

cells per 6-well plate and cultured for 8–10 days. Cells were stained with crystal violet stain after 8–10 days of culture and number of colonies were computed using countPHICS software. **(E)** Linear regression model for VPAC2 mRNA and Piwil2 mRNA from TCGA Pancreatic Cancer dataset (n=149). **(F)** Hallmarks GSEA analysis on differentially expressed genes (UP and DOWN) between parental and VPAC2KO Panc02 cells. For D, data are presented as bar graphs ± standard deviation (SD). For B and C, data are presented as + standard error (SEM). For B, one-way ANOVA test following by Dunnet's multiple comparison post-hoc test was performed. For C and D, two-tailed unpaired t test was used. *p<0.05, **p<0.01, ***p<0.001, ****p<0.0001.

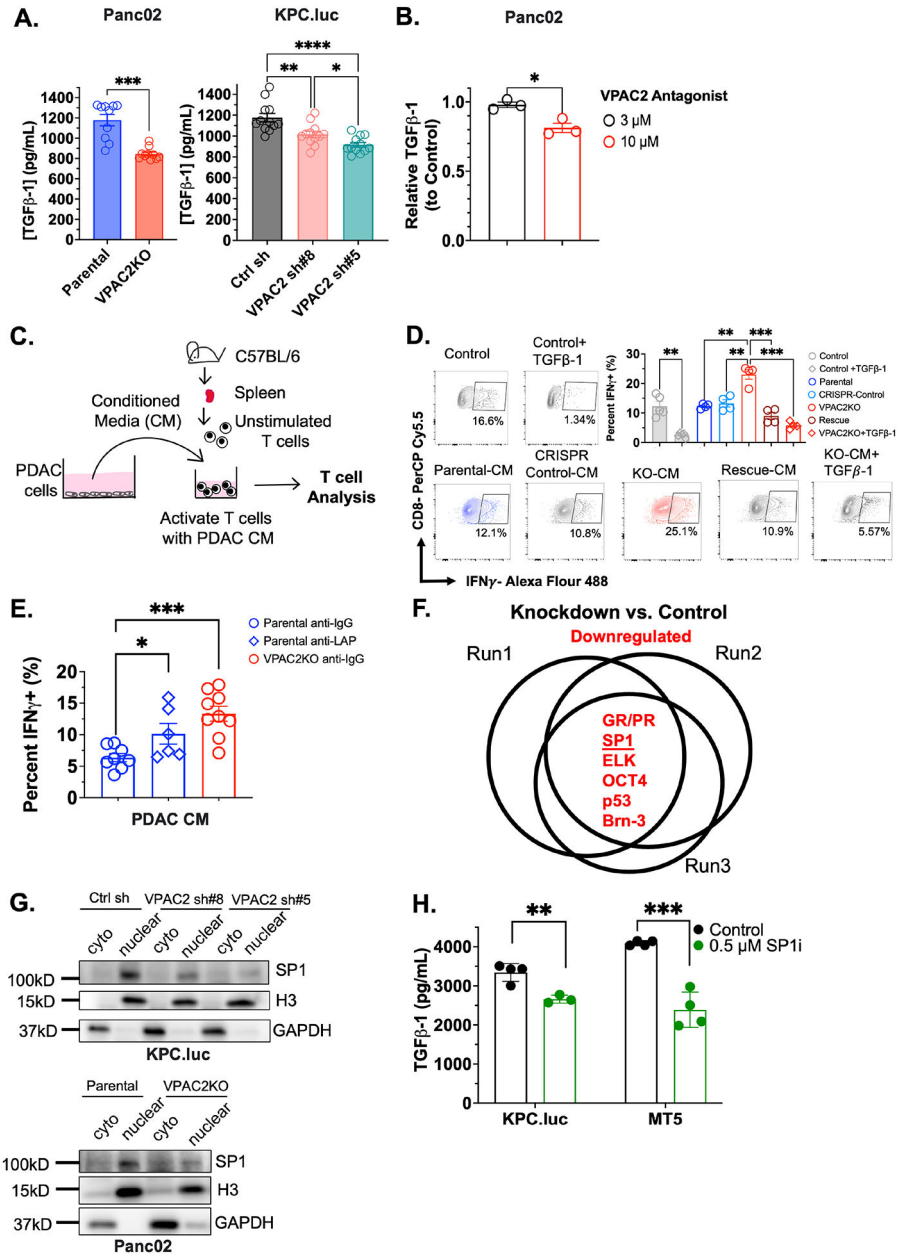

Figure 4.

Disruption of VPAC2 pathway leads to reduced TGFβ-1 via SP-1 and increased T cell function **(A)** Levels of secreted TGFβ-1 in Panc02 and KPC.luc cultures. CRISPR-KO or lentiviral knockdown of VPAC2 cells were compared to control cultures. **(B)** TGFβ-1 secretion in Panc02 upon treatment with 3 μM and 10 μM of VPAC2-antagonist for 3 days. **(C)** Schematic diagram for T cell assay performed with conditioned media from PDAC-cells. **(D)** Expression of IFNγ on CD8+ T cells following culture in conditioned media from parental, VPAC2KO, VPAC2-rescue Panc02 cells. Complete RPMI media was used as T cell control media. Recombinant TGFβ-1 at 2 ng/mL was added to conditioned media (CM) from VPAC2KO cells as additional group. T cells were stimulated with 1 μg/mL anti-CD3 coated plates and cultured for 48 hours. Golgi plug was added to culture 4 hours prior to

staining for IFNγ cytokine by flow cytometry (n=4–5). **(E)** Expression of IFNγ on CD8+ T cells following culture in TGFβ depleted conditioned media from parental. Anti-mouse LAP antibody conjugated with magnetic beads was used to deplete TGFβ from parental conditioned media. Anti-IgG was used as control antibody. **(F)** Venn diagram for commonly downregulated transcription factors between control and VPAC2 sh #8 KPC.luc cells (n=3). The downregulated transcription factors shown in red are ranked in order based on highest to lowest fold change, with SP1 ranking second (underlined). **(G)** Western blot validation of reduced SP1 expression in the nucleus of two VPAC2 sh clones (#8 and #5) in KPC.luc cells and VPAC2KO Panc02 compared control transduced and parental cells respectively. Histone 3 (H3) protein shown as loading control for nuclear extract and GAPDH for cytoplasmic extract. **(H)** Levels of secreted TGFβ-1 in KPC.luc and MT5 cell line following treatment with SP1 inhibitor, plicamycin, at 0.5 μM for 24 hours. For A, D, and E, data are presented as bar graphs ± standard error (SEM). For B, data are presented as ± standard deviation (SD). For A, and D, multiple unpaired t test with Welch's correction was used. For B, E and H, two-tailed unpaired t test was used. *p<0.05, **p<0.01, ***p<0.001, ****p<0.0001.

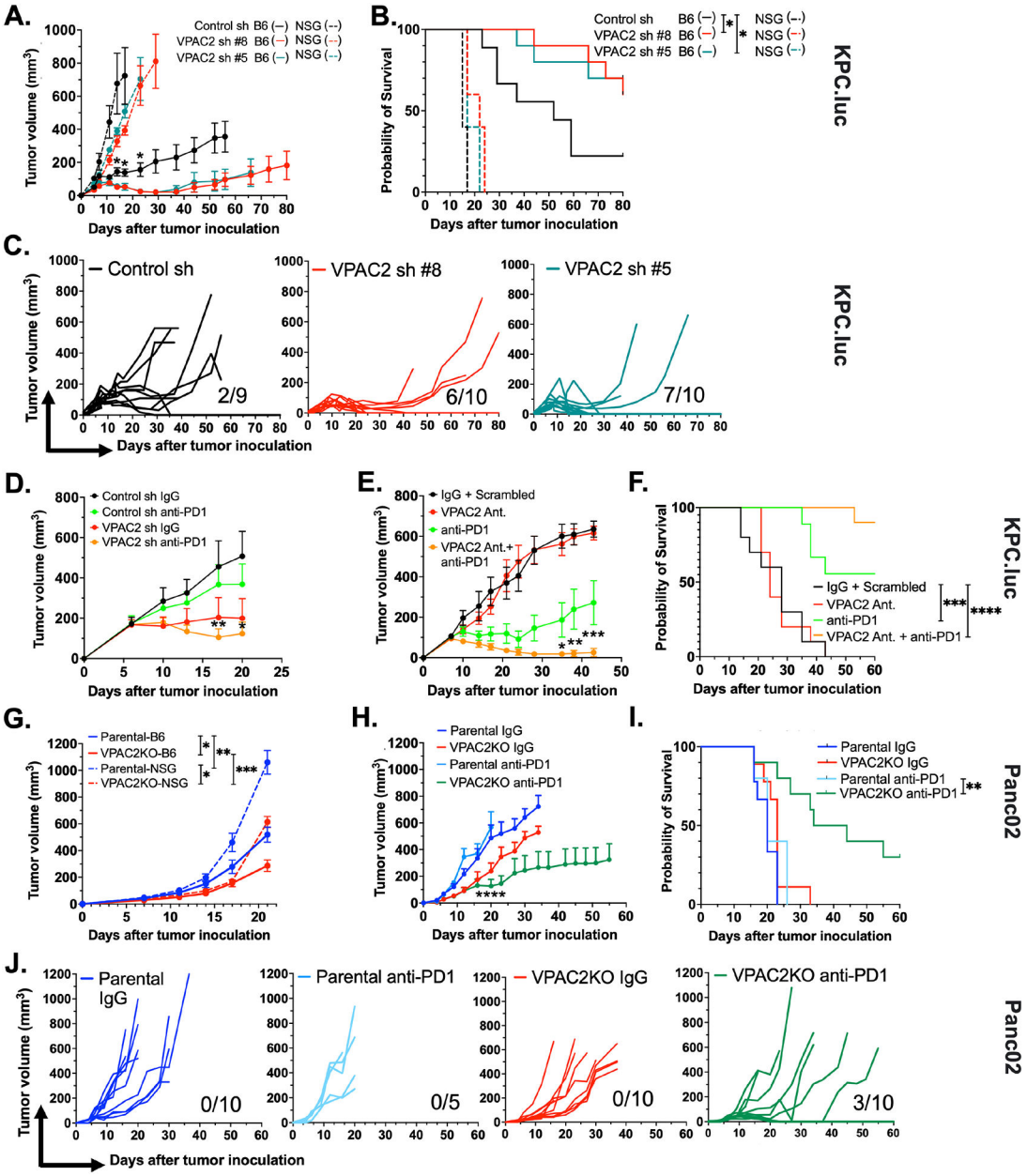

Figure 5.

Absence of VPAC2 leads to decreased tumor growth *in vivo* in a tumor cell intrinsic and cell-extrinsic manner in subcutaneous PDAC models. **(A)** Average tumor volume over time for control sh and VPAC2sh KPC.luc subcutaneously injected to C57BL/6 (n=9–10) (solid line) and to NOD SCID gamma (NSG) mice (n=5) (dashed line). **(B)** Survival plots for mice corresponding to A. **(C)** Spider plots showing tumor volume for individual C57BL/6 mouse injected with control (control sh, n=9) and VPAC2 knockdown (VPAC2 sh, n=10 each clone) KPC.luc cells (Top Panel). Numbers indicate the fraction of C57BL/6 mice that were tumor free at day 80 post tumor implantation. Average tumor volume over time for **(D)** control sh and VPAC2 sh KPC.luc injected to C57BL/6 and treated with isotype control (IgG) or anti-PD1 therapy (n=5); **(E)** Subcutaneous parental KPC.luc tumors in

C57BL/6 mice treated with VPAC2 antagonist (VPAC2 Ant.), anti-PD1 or combination of VPAC2 Ant. and anti-PD1 (n=9–10). Treatment was started at day 7 following tumor inoculation. VPAC2 antagonist was administered daily (20 μg, s.c.) and anti-PD1 (200 μg, IP) every 3–4 days for 10 days. **(F)** Survival plots for mice corresponding to E. **(G)** Average tumor volume over time for parental and VPAC2KO Panc02 cells subcutaneously injected to C57BL/6 (n=15–20) (solid line) and to NOD SCID gamma (NSG) mice (n=5) (dashed line). **(H)** Average tumor volume over time for parental and VPAC2KO Panc02 cells injected into male C57BL/6 (n=5–10) mice and treated with isotype IgG or anti-PD1 antibody. **(I)** Survival plots corresponding to H. **(J)** Spider plots showing tumor volume for individual male C57BL/6 mouse from H. Numbers indicate the fraction of C57BL/6 mice that were tumor free at day 60 post tumor implantation. Tumor volumes were measured by Vernier calipers one to two times a week until study endpoint. Data are presented ± standard error (SEM). For A, D, E, G and H, two-way ANOVA with Bonferroni correction was used. Log-rank test was used for statistical differences for survival curves. *p<0.05, **p<0.01, ***p<0.001, ****p<0.0001.

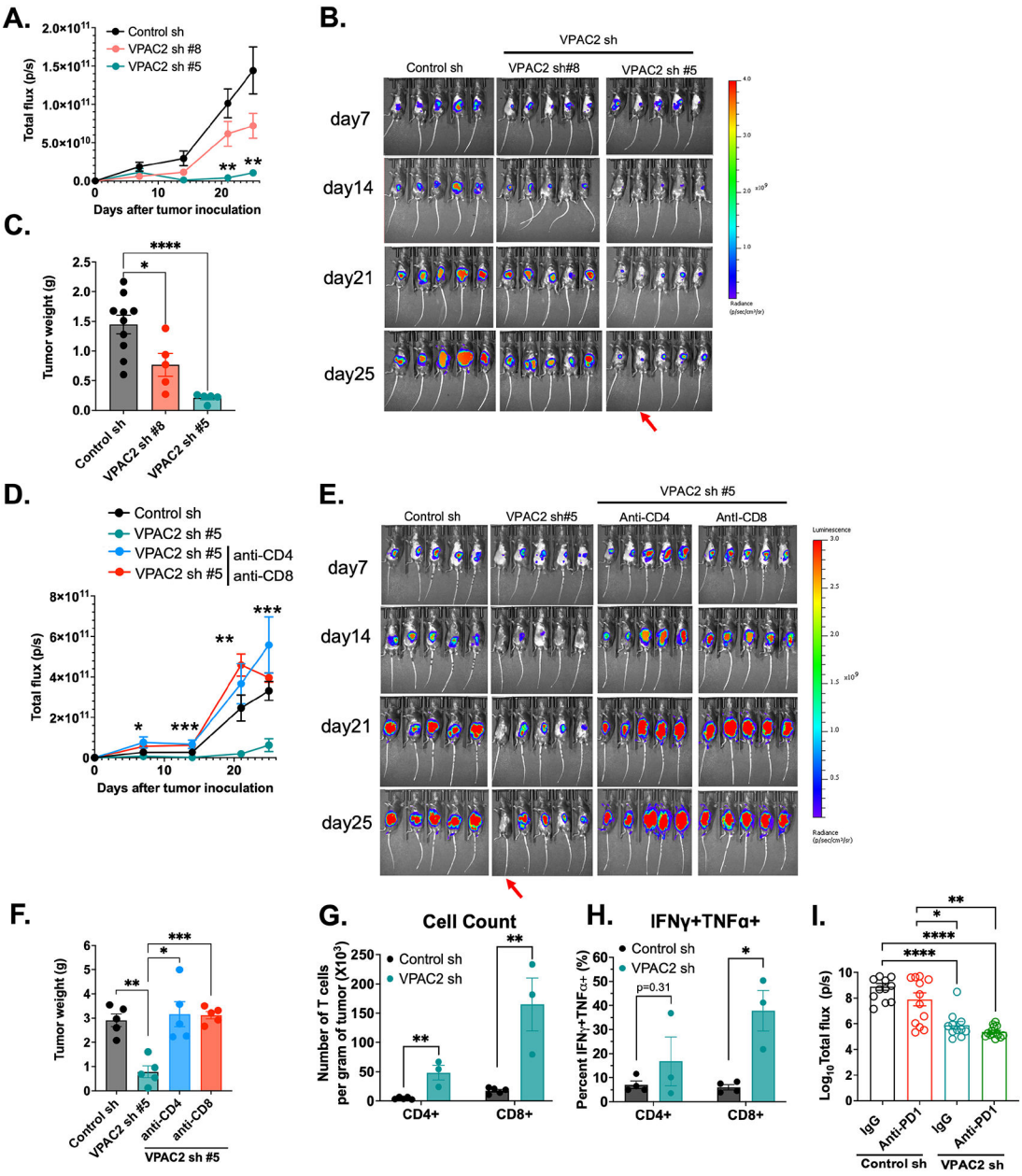

Figure 6.

Knockdown of VPAC2 on cancer cell reduces T cell dependent tumor burden in KPC.luc orthotopic model. Control sh and VPAC2 sh (#8 and #5) KPC.luc cells were surgically implanted in the tail of the pancreas of C57BL/6 mice. **(A)** Total photon flux was monitored over time by IVIS bioluminescent imaging. Isoflurane was used for anesthesia for bioluminescent imaging. **(B)** Pictures from IVIS bioluminescent imaging acquired weekly for the individual mice implanted with control or VPAC2 sh KPC.luc cells for 25 days. Red arrow indicates mice with minimal residual tumor at study end point. **(C)** Bar graph showing weight of tumor in grams on day 26 when the mice were euthanized. **(D)** C57BL/6 mice implanted with VPAC2 sh #5 clone KPC.luc receiving either monoclonal CD4 or CD8 monoclonal antibody compared to isotype treatment. Total flux from IVIS imaging

shown comparing the groups. **(E)** Pictures from IVIS bioluminescent imaging acquired weekly for the individual mice implanted with control or VPAC2 sh KPC.luc with isotype or anti-CD4/anti-CD8 blockade. Red Arrow indicating mice with minimal tumor residual at study end point. **(F)** Bar graph showing weight of tumor in grams on day 26 when the mice were euthanized corresponding to groups in D-E. Upon euthanasia, KPC.luc tumors were dissociated as single cells and analyzed for T cell count by flow cytometry. Bar plot showing **(G)** percent of T cell count as gated on CD4+ or CD8+ per gram of tumor **(H)** percent of T cells at the tumor expressing both IFNγ and TNFα upon 4 hours stimulation with leukocyte activation cocktail stimulation *ex vivo*. **(I)** Bar plot showing $\log_{10}$ total tumor flux (p/s) at day 26 following tumor implantation. All data are presented as ± standard error (SEM). For A, and D, two-way ANOVA with Bonferroni correction was used. For C, F, and I, one-way ANOVA test following by Dunnet's multiple comparison post-hoc test was used. For G and H, two-tailed unpaired t-test was performed. *p<0.05, **p<0.01 and ***p<0.001, ****p<0.0001.

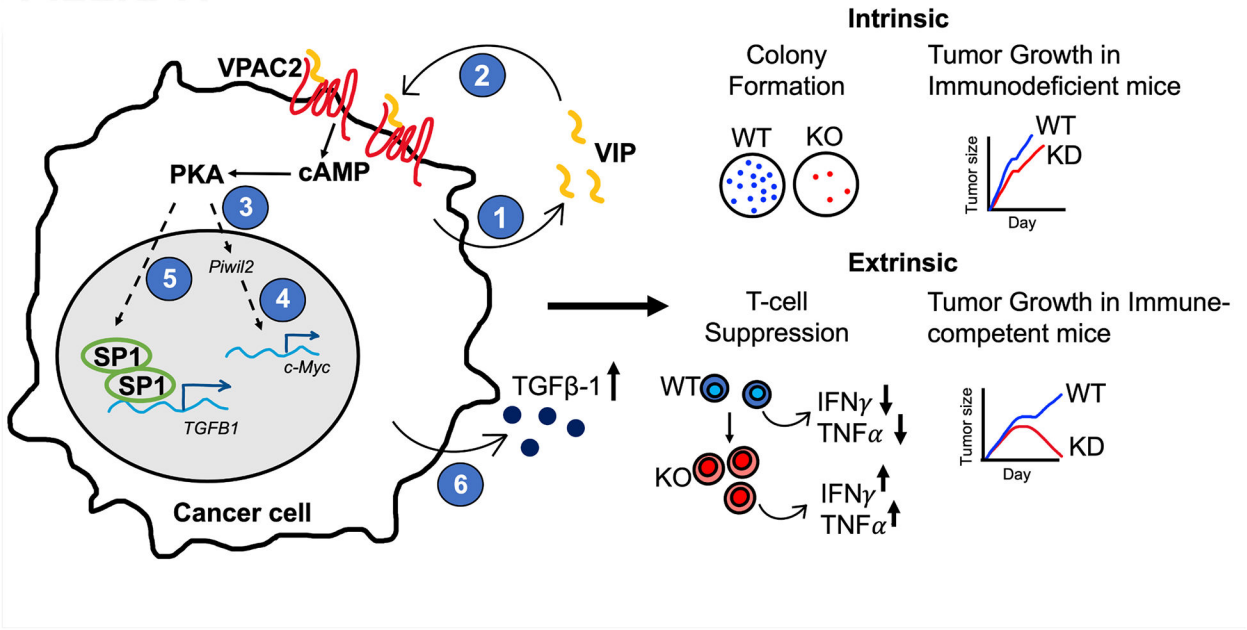

Figure 7.

Proposed model showing VPAC2 signaling on PDAC cells driving tumor-intrinsic and tumor-extrinsic effects. **(1)** Pancreatic cancer cells overexpress VIP and, **(2)** VIP binds to the VIP receptor, VPAC2, in an autocrine manner. Signaling via VPAC2 receptor leads to **(3)** increased Piwil2 expression that promotes tumor cell growth by driving **(4)** expression of c-myc and its targets. In addition, VPAC2 signaling (5) increases activity of SP1 in the nucleus to drive **(6)** TGFβ-1 expression leading to tumor cell extrinsic effects that suppress T cells contributing to immune escape in the tumor microenvironment. Dotted arrows represent undetermined pathways. Representative findings from experiments utilizing wild type (WT, blue) and VPAC2 knockout (KO, red) or knockdown (KD, red) are summarized to the right.